Optics Letters

Tunable silicon integrated quantum light source with on-chip FSR-free filters

Zhanping Jin,[1] Qirui Ren,[1] Dongning Liu,[1] Xiaosong Ren,[1] Yidong Huang,[1,2] and Wei Zhang[1,2,*]

[1]Frontier Science Center for Quantum Information, Beijing National Research Center for Information Science and Technology (BNRist), Department of Electronic Engineering, Tsinghua University, Beijing, China
[2]Beijing Academy of Quantum Information Sciences, Beijing, China
*zwei@tsinghua.edu.cn

Received 25 June 2024; revised 21 August 2024; accepted 15 October 2024; posted 16 October 2024; published 5 November 2024

In this work, we design and fabricate a telecom band quantum light source (QLS) on a silicon photonic chip, which integrates a piece of a long silicon waveguide as the nonlinear medium for spontaneous four-wave mixing (SFWM) and five narrow FSR-free bandpass filters based on a grating-assisted contra-directional coupler (GACDC). Two optical filtering functions of the silicon integrated QLS have been demonstrated. First, the QLS supports two tunable outputs of photon pair generations by four GACDC filters. A wavelength tunable range of 6 nm is demonstrated. Second, one GACDC bandpass filter is designed as an on-chip pump filter before the silicon waveguide. The performances of the QLSs with and without the on-chip pump filter are measured and compared. It shows that the on-chip pump filter has the effect to enhance the performance of the QLS by suppressing the Raman noise photons generated when a pump light propagated in optical fibers before it is injected into the chip. These results show that FSR-free filters would play important roles in developing silicon integrated QLSs.

https://doi.org/10.1364/OL.533799

In recent years, fiber-based quantum communication has exhibited a trend toward multi-user network [1,2]. Quantum entanglement distribution networks can implement networks with complex logical topologies by a simple star-type physical architecture, showing great potential on large-scale quantum networks [3–5]. Fiber-based quantum networks commonly employ wavelength division multiplexing (WDM) technology; the wavelength tunability of quantum entanglement resources would introduce new network functions. Therefore, the development of quantum network requires high-performance, compact, and tunable quantum light sources (QLSs) in a telecom band. Photon pair generation by spontaneous four-wave mixing (SFWM) in silicon waveguides is a promising way to develop such QLS as a silicon photonic chip [6]. A plenty of photonic components have been developed on a silicon photonic chip and used to generate various biphoton states [7–11]. Since the spectrum of photon pairs generated in silicon waveguides is very broad [12], optical filters are always required to select the signal and idler photons at specific wavelengths. To simplify the QLSs by integrating more functions on the chip, Mach–Zehnder interferometers and ring resonators are used to separate signal and idler photons [13–15]. Besides, micro-ring resonators are cascaded to realize bandpass optical filters with high extinction ratios up to 95 dB [16,17]. However, these optical filters have periodic filtering profiles in their transmission spectra, and their free spectral ranges (FSRs) are usually far smaller than the bandwidth of photon pairs generated in silicon waveguides by SFWM. Consequently, off-chip narrowband bandpass filters are still required to complete the filtering function. To fully integrate the filtering function for the signal and idler photons on the chip, integrated FSR-free filters should be introduced in silicon integrated QLSs. Especially, multiple tunable outputs of photon pairs could be supported by an array of tunable FSR-free filters. On-chip FSR-free filters are also helpful to reduce the noise photons of QLSs. It is well-known that the pump light of a silicon QLS should be filtered by optical filters with high extinction ratio to eliminate noise photons at the wavelengths of signal and idler photons. Usually, the filter for the pump light is built by commercial telecom filters with fiber pigtails. The pump light output from the fiber pigtail is then injected into the silicon chip by a lensed fiber or one of the fibers in a fiber array (FA). In this process, noise photons at the wavelengths of signal and idler photons would be generated by spontaneous Raman scattering in these fibers [18], which could not be suppressed in the following filters. It can be expected that an on-chip pump filter before the silicon waveguide could reduce these noise photons. However, the above functions of on-chip FSR-free filters on silicon integrated QLSs have not been explored and demonstrated to our knowledge.

In this Letter, we demonstrate a telecom band QLS on a silicon photonic chip integrating a long silicon waveguide as the nonlinear medium for SFWM and five FSR-free narrowband filters. The filters are based on grating-assisted contra-directional couplers (GACDCs) [19,20]. Four of them are located after the long silicon waveguide and used to select signal and idler photons, supporting the outputs of two sets of correlated photon pairs with different wavelengths. The wavelengths of each set are tunable by corresponding filters. Besides, one filter is located before the long silicon waveguide, which is used to suppress the

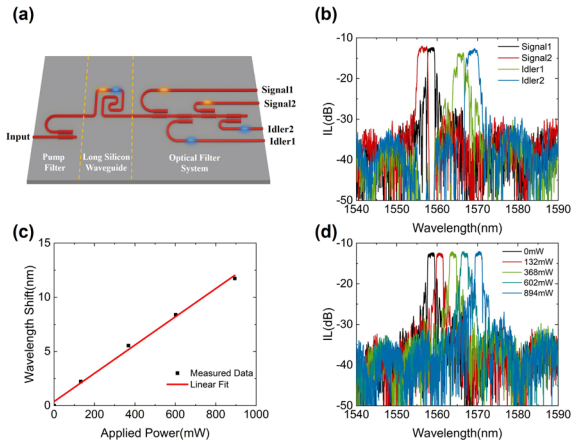

Fig. 1. (a) Schematic of the proposed integrated QLS. (b) Measured transmission spectra at the four output ports. (c) Measured center wavelength tuning of a specific GACDC filter. (d) Measured transmission spectra under different voltages.

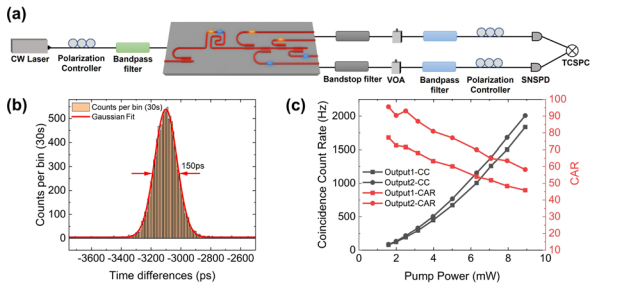

Fig. 2. (a) Schematic of the experimental setup of the photon pair generation. (b) Typical coincidence peak of Output 1. The histogram shows the counts per bin in 30 s; the red line is the Gaussian fit. (c) Coincidence count rates and CARs of the two outputs under different pump levels.

Raman noise photons generated when the pump light propagates in optical fibers before it is injected into the chip.

The schematic of the integrated QLS is shown in Fig. 1(a). The optical circuit on the chip can be divided into three parts: the pump filter, the long silicon waveguide, and the optical filter system for selecting signal and idler photons. The input pump light injects into the chip through a piece of fiber and passes through the narrowband pump filter based on a GACDC. The GACDC consists of two pieces of silicon waveguides with different widths and gratings formed by sidewall corrugations. One of them has a width of 600 nm and its corrugation width is 40 nm; the other has a width of 350 nm and its corrugation width is 60 nm. The gap of the two waveguides is 350 nm. The period of the corrugations in both waveguides is 328.4 nm. The phase matching between the two waveguides is achieved at the pump light wavelength by the sidewall corrugations; it enables the mode coupling from the quasi-TE mode of the input waveguide to the reverse-propagating quasi-TE mode of the output waveguide [21]. The pump filter removes the noise photons generated by the spontaneous Raman scattering when the pump light propagates in the optical fibers before the chip. Then, the pump light passes through the long silicon waveguide, which is 12 mm in length. During the pump light propagating, broadband signal and idler photons are generated by SFWM. The generated photons at specific wavelengths are selected by the optical filter system with four GACDC filters. These GACDCs have the same waveguide widths and corrugation widths with the narrowband pump filter. However, the periods of the corrugations of these GACDC are 327.2 nm, 326.4 nm, 329.5 nm, and 330.4 nm, respectively, leading to different filtering wavelengths. The output ports of the four GACDC filters are denoted by "Signal 1," "Signal 2," "Idler 1," and "Idler 2," respectively. All the filters based on the GACDC have electrical heater to tune their center wavelengths. Two sets of photon pairs are extracted and output from the chip, and their wavelengths are tunable. It is worth noting that a QLS sample without the pump filter is also fabricated on the same chip for comparison, which only has the long silicon waveguide and the optical filter system. At the ends of input and output silicon waveguides on the chip, spot size converters (SSCs) are fabricated to reduce the coupling loss between the silicon photonic chip and optical fibers. The silicon photonic chip of the QLS is fabricated on an SOI substrate with a 220 nm top-silicon layer (by Tianjin H-Chip Technology Group Corporation, China). The optical alignment between the silicon photonic chip and the fiber array (FA) is achieved by the auto-alignment system, and they are fixed by a UV adhesive. The silicon photonic chip is attached on a printed circuit board (PCB). The electrical connections between the pads on the chip for the electrical heater on the filters and the pads on the PCB are achieved by wire bonding using aluminum wires. The silicon photonic chip and the PCB are set on a thermoelectric cooler (TEC); their temperature is maintained at 15°C. Voltages are applied to the electrical heater on the chip through a multi-channel digital-to-analog converter (DAC).

The properties of the silicon photonic chip, especially the performance of the GACDC filters, are measured using the QLS sample without the pump filter. The light from a tunable laser (Santec TSL-570) is injected into the input waveguide of the QLS for the pump light, and the transmission spectra of the quasi-TE mode are measured at the four output ports from the four GACDC filters. The results are shown in Fig. 1(b). It can be seen that the transmission spectra of all the output ports show a feature of narrowband optical filtering with a bandwidth about 2 nm. Their center wavelengths are 1556.6 nm, 1558.5 nm, 1565.9 nm, and 1568.7 nm when the four GACDC filters do not have thermal control. The difference in their filtering profiles is likely due to fabrication imperfections. The insertion losses in the passbands of the four ports are close, about 14 dB. Specifically, the coupling loss between the chip and fibers is about 6 dB (two facets), the transmission loss of the long silicon waveguide is about 6 dB, and the insertion loss of a GACDC filter is about 2 dB, respectively. We apply different voltages on the electrical heaters on these GACDC filters to characterize their wavelength tuning range. A typical result of a specific filter (Signal 1) is shown in Fig. 1(c). It can be seen that the power efficiency of the center wavelength tuning is about 76.9 mW/nm, and a maximum tuning range of 11.7 nm is achieved in the measurement. Figure 1(d) is the measured transmission spectra under different applied voltages, showing that the filtering profile and extinction ratio are well maintained during the tuning range.

The performance of the photon pair generation of the QLSs is measured to show the effects of the FSR-free optical filters. The experimental setup is illustrated in Fig. 2(a). The pump laser is generated by the tunable laser at a fixed wavelength of 1563.86 nm. A fiber polarization controller is used to adjust the polarization state of the pump light to ensure that the pump

Table 1. Wavelength Configurations of the QLS

No.	λ_{signal} (nm)	λ_{idler} (nm)	$\Delta\lambda$(nm)
1	1561.863	1565.863	2
2	1559.863	1567.863	4
3	1557.863	1569.863	6
4	1555.863	1571.863	8

light is coupled to the quasi-TE mode of the silicon waveguide. A narrowband bandpass filter consisting of cascaded dense wavelength division multiplexers (DWDMs) with fiber pigtails is used to eliminate the noise photons of the pump light at the signal and idler wavelengths. When the pump light enters the chip, it excites SFWM in the long silicon waveguide and generates correlated photon pairs in a broad wavelength range. The photon pairs at specific wavelengths are selected by the on-chip optical filter system and output through a fiber array. The output signal and idler photons are subsequently pass through a narrowband band-stop filter consisting of cascaded DWDMs to remove the residual pump light and a broadband bandpass filter to eliminate the noise photons generated by the spontaneous Raman scattering in the silicon waveguide [22]. After these filtering processes, they are detected by superconducting nanowire single-photon detectors (SNSPDs, PHOTEC, China) and recorded by a time-correlated single-photon counter (TCSPC, Time Tagger Ultra, Swabian Instruments, Germany). Since the efficiencies of SNSPDs are polarization dependent, polarization controllers are required before the SNSPDs to optimize the polarization state of the detected photons. It is worth noting that there is no discrete narrowband bandpass filter in the setup since they have been integrated on the chip.

As shown in Fig. 1(a), the QLS supports two sets of outputs for the photon pair generation. The ports of "Signal 1" and "Idler 1" support the output denoted by "Output 1," and the ports of "Signal2" and "Idler2" support the output denoted by "Output 2," respectively. According to the pump wavelength and tuning ranges of center wavelengths of the GACDC filters for these ports, we set four wavelength configurations of the output photon pairs; their signal and idler wavelengths (λ_{signal} and λ_{Idler}) are shown in Table 1. The space between the signal/idler wavelengths and the pump wavelength is denoted by $\Delta\lambda$. It is worth noting that the two sets of outputs should have different wavelength configurations, since their output photon pairs are from the same silicon waveguide. Consequently, there are 12 combinations of the wavelength configurations for the two outputs.

To show the function of multiple tunable wavelength outputs supported by the four GACDC filters, the performance of the photon pair generation of the two outputs is measured under all the 12 combinations of the wavelength configurations. Figures 2(b) and 2(c) show the experimental results when Outputs 1 and 2 are set to wavelength configurations 2 and 3, respectively. A typical coincidence peak of Output 1 is shown in Fig. 2(b) when the pump power is set to 6 mW, showing a clear quantum correlation between the signal and idler photons. The full width at half maximum (FWHM) of the coincidence peak is about 150 ps. The coincidence count rates and coincidence-to-accidental coincidence ratios (CARs) of the two outputs under different pump levels are measured and shown in Fig. 2(c). The width of the coincidence window in these measurements is set to 200 ps, which covers most of the coincidence peak. The maximum coincidence rate of Output 1 is about 1.8 kHz, with a CAR of 45.8.

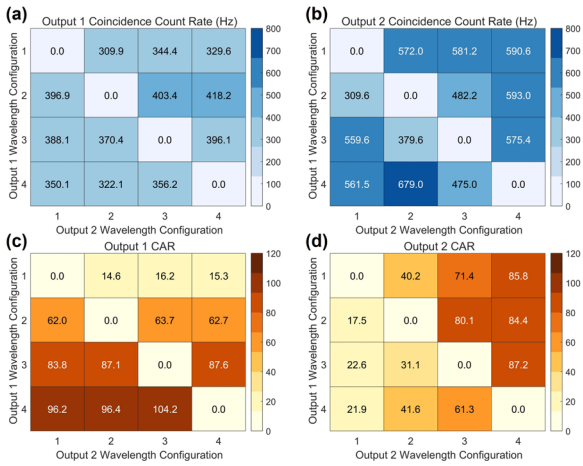

Fig. 3. Results of the photon pair generation of the two outputs under different combinations of wavelength configurations. The coincidence count rates of Outputs 1 and 2 are shown in (a) and (b). The CARs of Outputs 1 and 2 are shown in (c) and (d). Each square in these figures represents a combination of wavelength configurations of the two outputs. The values of experimental results are shown by the shades of color.

That of Output 2 is about 2 kHz with a CAR of 58.2. Experimental results show that both two outputs support the correlated photon pair generation at their wavelength configurations.

The performance of the photon pair generation of the two outputs under different combinations of wavelength configurations is shown in Fig. 3. Figures 3(a) and 3(b) are the results of coincidence count rates of Outputs 1 and 2, respectively. The measured CARs of Outputs 1 and 2 are shown in Figs. 3(c) and 3(d). Each square in these figures represents a combination of wavelength configurations of the two outputs, which are indicated by the bottom and left labels. The values of these experimental results are shown by the shades of color. It can be seen that the coincidence counts can be measured at both outputs under all the combinations. The differences of coincidence count rates of Output 1 under different combinations are small, but those of Output 2 are relatively large. It can be explained that the filters of Output 1 are before those of Output 2 in the on-chip optical circuit; hence, the performance of Output 2 would be impacted by the filters of Output 1. On the other hand, the measured CARs show a large difference. For both outputs, a smaller CAR would be measured if the photon pairs are generated under a wavelength configuration with smaller space between signal/idler wavelengths and pump wavelengths and vice versa. It is due to the insufficient pump light suppression of the off-chip band-stop filter and the nonideal profiles of the transmission spectra of the on-chip GACDC filters. The experimental results in Fig. 1(b) show that for a specific wavelength out of the passband of the filter, a smaller extinction would be expected if the space between it and the pump wavelength is smaller. Hence, the photon pairs under the wavelength configuration with smaller wavelength difference would be more impacted by the noise photons of the residual pump light. This effect could be avoided by further optimization of the on-chip and off-chip filters. On the whole, the experimental results in Fig. 3 demonstrates that the QLS has two tunable outputs of the photon pair generation, which is supported by the four FSR-free filters on-chip.

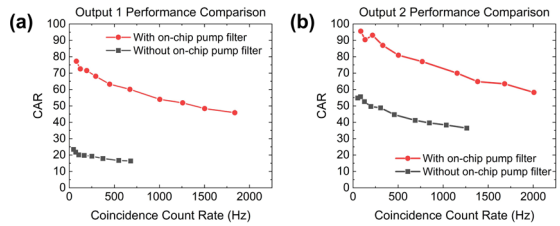

Fig. 4. Performance comparison of two QLSs with and without the on-chip pump filter. (a) and (b) Experimental results of Outputs 1 and 2 of the two QLSs. The red circles and black squares are the measured CARs of the QLSs with and without the on-chip filter, respectively.

In the QLS, another FSR-free filter is designed before the silicon waveguide to suppress noise photons generated by the spontaneous Raman scattering when the pump light propagates in optical fibers before it is injected into the chip. To demonstrate this effect, two QLSs with similar optical circuits are fabricated: one has the on-chip pump filter before the silicon waveguide as shown in Fig. 1 and the other does not. The insertion loss of the pump filter is about 2 dB estimated by previous measurements. The performances of these two QLSs are measured and compared to show the effect of the FSR-free filter. In these measurements, Outputs 1 and 2 are set to wavelength configurations 2 and 3, respectively, for both QLSs. The experiment shows that the coincidence count rates of both outputs of the QLS with the pump filter are a little higher than those of the QLS without the pump filter under the same pump power. It is mainly due to the difference of the coupling losses between optical fibers and the chips for the two QLSs. To remove the impact of the coupling losses and show the effect of the on-chip pump filter more clearly, we compare the CARs under the same coincidence count rates. The experimental results are shown in Fig. 4. Figure 4(a) is the measured CARs of Output 1 in the two QLSs with increasing coincidence count rates, and those of Output 2 in the two QLSs are shown in Fig. 4(b). It can be seen that the CAR of Output 1 increases from 16.3 to 60.9 (3.74-fold increase) due to the pump filter under coincidence count rates of ~700 Hz. Similarly, the CAR of Output 2 increases from 38 to 70 (1.84-fold increase) under coincidence count rates of ~1 kHz. Both results show the effect of the FSR-free filter on the noise photon suppression.

In summary, we demonstrate a telecom band QLS on a silicon photonic chip integrating a piece of a long silicon waveguide as the nonlinear medium for SFWM and five GACDC narrow bandpass filters. Thanks to their FSR-free filtering profiles, two optical filtering functions of the silicon integrated QLS have been demonstrated. First, the QLS supports two tunable outputs of photon pair generations by four GACDC bandpass filters. A wavelength tunable range of 6 nm is demonstrated at both outputs. The tunable range of the QLS is limited by the low tuning efficiency of the GACDC, which could be improved by incorporating deep trenches around the GACDCs to provide thermal isolation and reducing the buffer silicon oxide layer below the electrical heater. Second, one GACDC bandpass filter is designed as an on-chip pump filter before the long silicon waveguide. The performances of the photon pair generation of the QLSs with and without the on-chip pump filter are measured and compared. It shows that the on-chip pump filter, which is FSR-free, has the effect to enhance the performance of the silicon integrated QLS by suppressing the Raman noise photons generated when the pump light propagated in optical fibers before it is injected into the chip. These experimental results show that the GACDC narrow bandpass filters are promising candidates as on-chip FSR-free filters in silicon integrated QLSs. It is worth noting that the tunable range of the QLS is limited by the low tuning efficiency of the GACDC which can be mitigated by incorporating deep trenches around the GACDCs to provide thermal isolation and reducing the buffer silicon oxide layer below the electrical heater. Due to limited extinction ratio of these on-chip filters, the off-chip filters are still required to eliminate the residual pump light and noise photons from the spontaneous Raman scattering in the silicon waveguide in this work. To integrate all the optical filtering functions on the silicon chip, the extinction ratio of the GACDC filters should be improved by optimizing the filter design and fabrication. Their extinction ratio could be further improved by filter cascading. Besides, high-performance band-stop filters [23,24] could be introduced before the GACDC filters to achieve sufficient suppression for the pump light.

Funding. National Key Research and Development Program of China (2023YFB2806700); National Natural Science Foundation of China (92365210); Tsinghua Initiative Scientific Research Program; Tsinghua University-Zhuhai Huafa Industrial Share Company Joint Institute for Architecture Optoelectronic Technologies (JIAOT).

Disclosures. The authors declare no conflicts of interest.

Data availability. Data underlying the results presented in this Letter are not publicly available at this time but may be obtained from the authors upon reasonable request.

REFERENCES

1. S. Wehner, D. Elkouss, and R. Hanson, Science **362**, eaam9288 (2018).
2. S.-H. Wei, B. Jing, X.-Y. Zhang, *et al.*, Laser Photonics Rev. **16**, 2100219 (2022).
3. X. Liu, J. Liu, R. Xue, *et al.*, PhotoniX **3**, 2 (2022).
4. S. Wengerowsky, S. K. Joshi, F. Steinlechner, *et al.*, Nature **564**, 225 (2018).
5. D. Liu, J. Liu, X. Ren, *et al.*, Photonics Res. **11**, 1314 (2023).
6. L. Caspani, C. Xiong, B. J. Eggleton, *et al.*, Light: Sci. Appl. **6**, e17100 (2017).
7. J. W. Silverstone, D. Bonneau, K. Ohira, *et al.*, Nat. Photonics **8**, 104 (2014).
8. N. Lv, W. Zhang, Y. Guo, *et al.*, Opt. Lett. **38**, 2873 (2013).
9. C. Ma, X. Wang, V. Anant, *et al.*, Opt. Express **25**, 32995 (2017).
10. K.-I. Harada, H. Takesue, and H. Fukuda, Opt. Express **16**, 20368 (2008).
11. H. Takesue, H. Fukuda, T. Tsuchizawa, *et al.*, Opt. Express **16**, 5721 (2008).
12. L. Yu, C. Yuan, R. Qi, *et al.*, Photonics Res. **8**, 235 (2020).
13. J. C. Adcock, C. Vigliar, R. Santagati, *et al.*, Nat. Commun. **10**, 3528 (2019).
14. D. Llewellyn, Y. Ding, I. I. Faruque, *et al.*, Nat. Phys. **16**, 148 (2020).
15. S. Paesani, Y. Ding, R. Santagati, *et al.*, Nat. Phys. **15**, 925 (2019).
16. R. R. Kumar and H. K. Tsang, Opt. Lett. **46**, 134 (2021).
17. C. M. Gentry, O.S. Magaña-Loaiza, M. Wade, *et al.*, in *Conference on Lasers and Electro-Optics* (IEEE, 2018).
18. Q. Lin, F. Yaman, and G. P. Agrawal, Phys. Rev. A **75**, 023803 (2007).
19. H. Qiu, J. Jiang, P. Yu, *et al.*, J. Lightwave Technol. **36**, 3760 (2018).
20. W. Shi, X. Wang, C. Lin, *et al.*, Opt. Express **21**, 3633 (2013).
21. W.-P. Huang, J. Opt. Soc. Am. A **11**, 963 (1994).
22. J. I. Dadap, R. L. Espinola, R. M. Osgood, *et al.*, Opt. Lett. **29**, 2755 (2004).
23. N. C. Harris, D. Grassani, A. Simbula, *et al.*, Phys. Rev. X **4**, 041047 (2014).
24. D. Oser, F. Mazeas, X. Le Roux, *et al.*, Laser Photonics Rev. **13**, 1800226 (2019).